4

Egypt. J. Chem. **Vol. 64**, No.1. pp. 33 - 45 (2021)

Effect of Preparation Parameters and Sintering Conditions on the Properties and Microstructure of Nickel Pellets Prepared by Conventional Powder Metallurgy

Lamiaa Z. Mohamed[a],*, Omayma A. El kady[b], Mohamed. M. Lotfy[a], Hafiz A. Ahmed[a], Fawzi A. Elrefaie[a]

[a]*Mining, Petroleum, and Metallurgical Engineering Dept., Faculty of Engineering, Cairo University, Egypt.*

[b]*Powder Technology Division, Central Metallurgical Research and Development Institute (CMRDI), Helwan, Egypt.*

Abstract

Eleven types of nickel pellets were prepared from two types of nickel powders. The first type of Ni powder had filamentary particles in shape with particle size less than 63 µm, the second type of Ni powder possessed nearly spherical particles in shape with particle size less than 149 µm. One type of pellets was prepared from Ni(B) powder whose particle size was reduced to less than 70 µm. The pellets were fabricated by conventional powder metallurgy. Green pellets were initially formed by compaction under 420 MPa and then sintered at 1200 °C. The dependence of the characteristics and microstructure of sintered pellets on particle shape, size of particles, powder milling, binder addition, holding time at 1200 °C, and the rate of raising green pellets temperature at the early stage of heating was investigated. Weighing in air and in floating liquid (water), measuring the sintered pellets volume, X-ray diffractometry, optical microscopy, scanning electron microscopy, X-ray energy dispersion analysis, and Vickers microhardness measurements were used to determine the properties and microstructures of fabricated pellets. The apparent density and microhardness of pellets prepared from filamentary particles with the addition of wax as a binder were the highest, about 8.23 gm/cm3 and 158 VHN, respectively.

Keywords: Nickel; Powder Metallurgy; Microstructure; Sintering; Density

1. Introduction

Nickel and nickel alloys are used for a wide variety of industrial applications [1]. For example, new advanced materials which are used at high-temperature applications because of their physical and mechanical properties and also due to their high oxidation resistance at high temperature, nickel-chromium composite used as a self-lubricant material for the aerospace technology [2], Rene95 Ni-based superalloys for turbine disk applications [3,4], oxide dispersion strengthening (ODS) Ni-based superalloys used in nuclear reactors and petrochemical industry[5], nickel disc alloys for applications under fatigue stresses [6] and complex net-shaped components [7]. The high-temperature oxidation characteristics of pure nickel pellets, which is the base metal of most of the alloys used in manufacturing the high temperature new advanced materials, represents a good base for understanding the behavior of high-temperature oxidation of Ni-base alloys. Most of the previous oxidation study on nickel was carried out on homogenous nickel with different impurity levels and at different conditions [8-11]. Therefore, there is a need for studying the oxidation characteristics of inhomogeneous nickel and nickel alloys to characterize the thermal stability of parts made from powder by compaction and sintering. Accordingly, the

main aim of this work is to study the effect of particles shape, size of particles, milling, the addition of wax as a binder, rate of raising green pellets temperature at the early stage of heating and holding time at the maximum sintering temperature on the properties

(measured apparent density and density measured by Archimedes method, estimated porosity and densification, and microhardness) and microstructure of sintered nickel pellets.

2. Experimental work
2.1 Material

Nickel pellets were prepared from filamentary nickel particles, Ni(A), whose particle size less than 63 µm (by screening) or from nearly spherical nickel particles, Ni(B), whose particle size less than 149 µm (partical size was given by the supplier Dop Company). One type of pellets was prepared from Ni(B) powder whose particle size was reduced to less than 70 µm. The chemical analysis of Ni(A) and Ni(B) are listed in Table 1. The main impurity in both nickel types was carbon. The characteristics of the powders of both nickel types were examined by using X-ray

diffractometry and scanning electron microscopy (SEM). The X-ray diffractometer model used for powder analysis is BROKERD8- with Cu kα radiation (λ=0.15406 nm, 45 kV and 40 mA) made in Germany and located in- Central Metallurgical Research and Development Institute. The X-ray energy dispersive analyzer linked with scanning electron microscope model is FEI-Inspect S-Quanta 250 FEG, Holland and located in Housing and Building National Research Center (HBRC).

Table 1 The Chemical Analysis of Different Nickel Types in wt.%

Elements, %	C	S	Fe	Cu	Mn	Ni
Ni(A)*	0.06	--	0.01	0.001	0.0001	bal.
Ni(B)**	0.08	0.001	0.01	--	--	bal.

* The data is obtained by wet chemical analysis.
** The analysis is given by the supplier (Dop Company).

2.2 Pellets Preparation

Four different types of pellets were fabricated from Ni(A), types (I), (II), (III), and (IV). Seven different types were compacted and sintered from Ni(B), types (V), (VI), (VII), (VIII), (IX), (X) and (XI). The sintering vacuum furnace model is 121212-50, GEA/Vacuum Industry, USA and it is located in Central Metallurgical Research and Development Institute. The different heating programs used in this investigation were rapid heating program, P(1), medium heating program, P(2), and slow heating program, P(3). The heating steps of these programs are schematically shown in Fig. 1. The diagrams in Fig.1 indicate that the difference between the heating programs is observed only at the early stage of raising temperature from room temperature up to 300 °C. The composition, the preparation conditions, the used heating program, and the holding time at 1200 °C for each type of pellets are shown in Table 2. Green pellets were prepared by pressing particles under 420 MPa in a die with 20 mm inner diameter. The green pellets were then sintered at 1200 °C in a vacuum furnace under 10-3 torr. The diameter of obtained pellets

varied from 18.5 mm to 19.0 mm and their thickness varied from 3.5 mm to 3.7 mm. The sintered pellets of types (I) and (V) were manufactured from Ni(A) and Ni(B) powders, respectively, with the addition of 0.5 wt%Cr paraffin wax as a binder and employing the same preparation and sintering conditions. Pellets of type (I) and (II) were formed from Ni(A) powder, under the same preparation and sintering conditions with the addition of 0.5 wt% paraffin wax, except milling the Ni(A) powder used in preparing type (II) pellets for 4 h in a stainless steel ball mill using stainless steel balls with ball to powder ratio of 10:1. Pellets of types (V) and (VI) were prepared from type (B) particles under the same preparation conditions and sintering condition; however, the original Ni(B) powder with particle size less than 149 µm used in the preparation of type (V) while the size of particles of Ni(B) used in the preparation of type (VI) pellets was less than 70 µm due to milling the original Ni(B) powder for 1 h in a high-speed vertical ball mill at speed of 600 r.p.m. All other pellets were prepared without the addition of any wax. Types (VIII), (IX),

and (X) pellets were prepared from Ni(B) particles under the same conditions but with holding time of 1, 2, or 3 h at 1200 °C. Pellets of type (XI) were formed from Ni(B) particles similarly as pellets of type (IX) but with the different heating program, P(3). Pellets of type (III) and (VII) were prepared from Ni(A) and

Ni(B) particles, respectively, by employing the same preparation conditions and sintering conditions; the same was applied for pellets of types (IV) and (IX). Pellets of type (VII) were fabricated in a similar way such as pellets of type (V) but without the use of any binder.

Table 2 Materials and Preparation Conditions for Pellets of Different Types

Type	Materials	Preparation conditions
(I)	Ni(A) + 0.5wt% paraffin wax	$P_{(1)}$ -holding time is 1 hr
(II)	Ni(A) + 0.5wt% paraffin wax + milling* for 4 h	$P_{(1)}$ -holding time is 1 hr
(III)	Ni(A)	$P_{(1)}$ -holding time is 1 hr
(IV)	Ni(A)	$P_{(2)}$ -holding time is 2 hr
(V)	Ni(B) + 0.5wt% paraffin wax	$P_{(1)}$ -holding time is 1 hr
(VI)	Ni(B) + 0.5wt% paraffin wax + milling** for 1 hr	$P_{(1)}$ -holding time is 1 hr
(VII)	Ni(B)	$P_{(1)}$ -holding time is 1 hr
(VIII)	Ni(B)	$P_{(2)}$ -holding time is 1 hr
(IX)	Ni(B)	$P_{(2)}$ -holding time is 2 hr
(X)	Ni(B)	$P_{(2)}$ -holding time is 3 hr
(XI)	Ni(B)	$P_{(3)}$ -holding time is 2 hr

 * milling was carried out in a horizontal ball mill with speed 100 r.p.m
** milling was carried out in a vertical ball mill with speed 600 r.pm, the particle size of Ni(B) was reduced to less than 70 µm
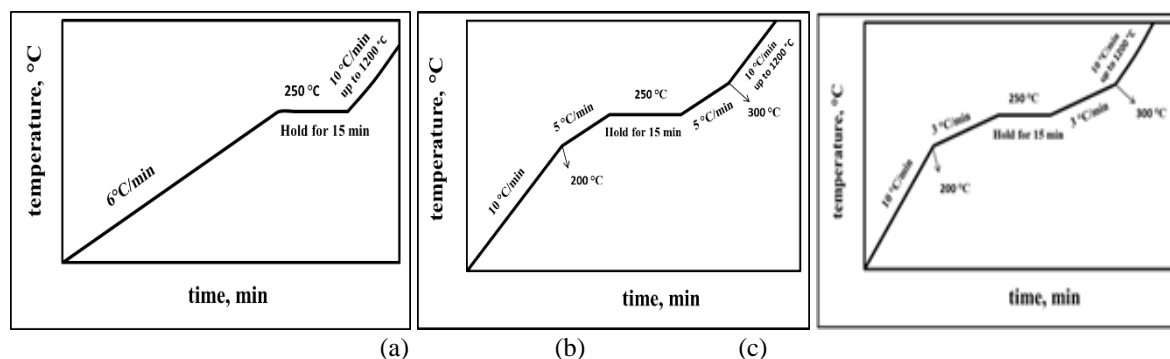

Fig. 1 Schematic figures for the rapid heating program, $P_{(1)}$ (a), the intermediate heating program, $P_{(2)}$ (b) and the slow heating program, $P_{(3)}$ (c)

Accordingly, the effect of particle shape, size, holding time at 1200 °C, the early stage of heating, wax addition or milling on the properties of sintered pellets could be obtained by comparing the experimentally determined values of densities as follows:

effect of particle size: (V and VI),

effect of particles shape: (I and VI),

effect of heating time: (VIII, IX, and X),

effect of the early stage of heating: ([IX and XI),

effect of wax addition: (I and III) and (V and VII),

effect of low-speed milling (the smaller size particles):   (I and II).

_____

Egypt. J. Chem. Vol. 64, No.1 (2021)

2.3 Density Measurements

The apparent density, ρapp, of sintered pellets was determined by estimating the ratio of the weight of each pellet in air to its volume. Besides, the density of sintered pellets was measured by Archimedes method, ρAr, using water as floating liquid and applying Eq. 1 where Wa and Ww are the weight of the pellet in air and water, respectively [12].

$$\rho Ar = Wa/ (Wa-Ww), \hspace{2cm} (1)$$

2.4 Phase Analysis, Microstructural Observation, and Elemental Detection

Phase analyses of the sintered pellets were examined by using X-ray diffractometry (XRD). The X-ray diffractometer model for pellets is X'Pert PRO PAN analytical diffractometer with Cu kα radiation- λ=0.15406 nm, 45 kV and 40 mA made in Netherlands and located in Central Metallurgical Research and Development Institute. For microstructural observation of a pellet, it was mounted and grinded successively with silicon carbide abrasive papers in grit size ranges from 100 to 800, and then polished with 0.3 µm alumina paste. The pellet was then etched in an aqueous solution containing 15 cm3 nitric acid (70 wt% HNO_3+30 wt% H_2O) and 90 cm3 acetic acid (99.5 wt% CH_3COOH) [13]. The microstructure of the etched pellets was then observed by optical and scanning electron microscopy. Elemental% indicators of carbon, oxygen, and nickel of a pellet were detected by employing X-ray energy dispersion analysis (EDAX) at different spots of the surface of the pellets. The optical microscope model is Olympus BX41M-LED and located in Mining, Petroleum and Metallurgical Engineering Department, Faculty of Engineering, Cairo University. The X-ray energy dispersive analyzer linked with scanning electron microscope model is FEI-Inspect S-Quanta 250 FEG, Holland and located in Housing and Building National Research Center (HBRC).

2.5 Microhardness Measurements

Vickers microhardness testing was utilized to measure the microhardness of each pellet by applying 1.96 N load for 10 sec. The model of the microhardness is 1600 Series Buehler and its location is Mining, Petroleum and Metallurgical Engineering Department, Faculty of Engineering, Cairo University. The measurements were taken at five different locations on each surface to estimate the average microhardness value.

3 Results and Discussion
3.1 Powder Characterization

The X-ray diffraction patterns of Ni(A) and Ni(B) powders were obtained between the angles 40º and 100º. The patterns are shown in Fig. 2; five peaks were detected in each pattern. The intensity of Ni(A) peaks was slightly higher than the corresponding peaks of Ni(B) which might due to the higher randomness of the smaller size of Ni(A) particles. The peaks coincided with those reported for pure nickel powder [14,15]. The five peaks on the pure Ni matched as in literature with miller indices (111), (200), (220), (311) and (222). This, in turn, signified the purity and crystallinity of both nickel powders.

Fig. 3 shows the powder morphology of Ni(A) and Ni(B). Filamentary Ni(A) powder has a larger surface area per unit volume than that of Ni(B) powder because of the smaller size of Ni(A) particles. Many of Ni(A) particles agglomerate with each other [16]. It might be due to the species in the environment promote adhesion between particle surfaces, agglomerates tend to be larger [16]. Each Ni(B) particle possessed a nearly spherical shape.

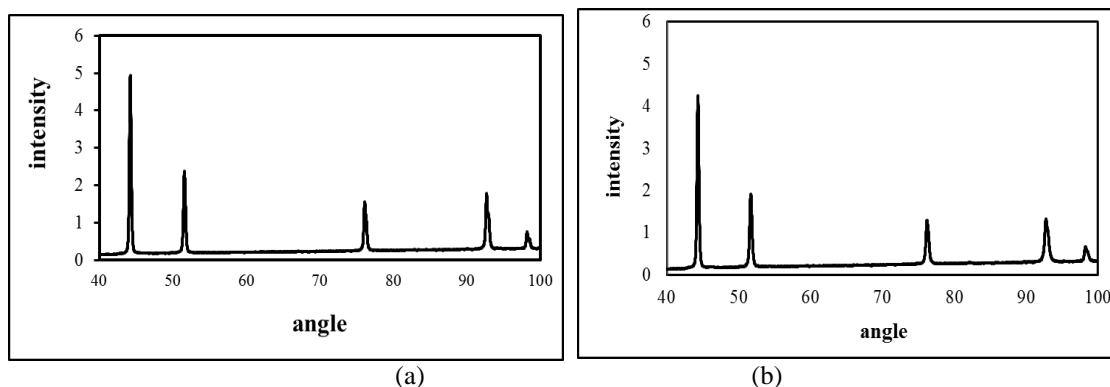_____

Egypt. J. Chem. **Vol. 64,** No.1 (2021)

Fig. 2 X-ray diffraction patterns of Ni (A) powder (a) and Ni (B) powder (b)
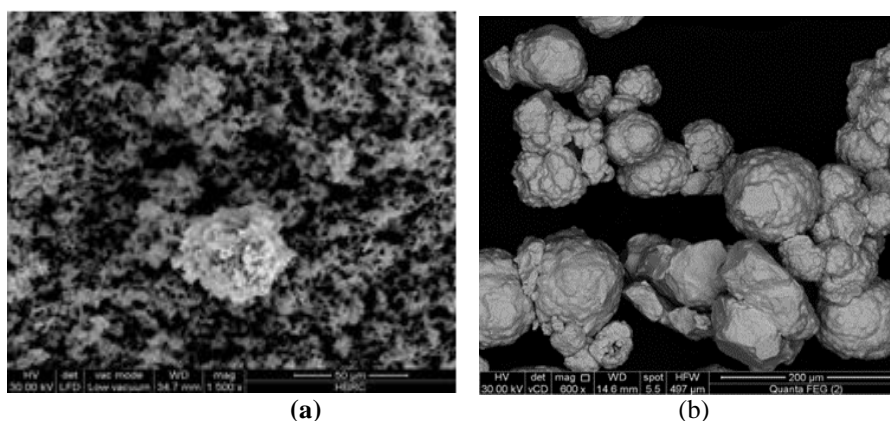

Fig. 3 Scanning electron images of Ni (A) powder (a) and Ni(B) powder (b)

3.2 Characteristics of Sintered Pellets
3.2.1 Apparent Density Measurements, and Estimation of Porosity and Densification

The values of measured ρapp and ρAr for sintered pellets are presented in Table 3.

Table 3 Measured Apparent and Archimedes Densities for Different Types of Nickel Pellets

Pellets type	ρ_{app}, g/cm^3	ρ_{Ar}, g/cm^3
(I)	8.24	8.69
(II)	8.23	8.77
(III)	7.43	8.33
(IV)	7.74	7.98
(V)	7.40	8.13
(VI)	7.70	8.30
(VII)	7.03	8.16
(VIII)	6.70	8.20
(IX)	7.35	8.30
(X)	7.50	8.33
(XI)	7.58	7.60

Table 3 indicates that the average values of ρapp for types (I) and (II) pellets prepared from Ni(A) with the addition of paraffin wax as a binder are relatively much higher than ρapp of sintered pellets prepared from Ni(A) powder without the addition of wax or from Ni(B) powder with or without the addition of wax, 6.70-7.58 g/cm3. The values of ρapp of pellets of types (I) and (II) were almost the same which, in turn, indicated that the milling in horizontal mill for 4 h had a negligible effect on prepared sintered pellets. The

_____

_____

higher ρapp of pellets that belong to types (I) and (II) might be due to the filamentary smaller size particles. The smaller size particles possessed higher surface area per unit volume and thus raising the compatibility of the powder and sintering rate [16,17]. The utilization of a binder might have a positive effect also on the sintering rate.

Tables 3 also indicate that the values of ρapp, for pellets of types (VIII), IX), and (X) were getting higher with increasing the holding time at 1200 °C. This is anticipated since the particles begin to grow together by necking at the initial stage of sintering and

then the grains start to grow via lattice diffusion during the intermediate sintering stage and finally, the continuous pores start to become discontinuous [16, 18]. According to the different models, the sintering rate decreases with time [18]. This, in turn, explained the smaller difference in density values between pellets of types (IX) and (X) than that of pellets of types (VIII) and (IX).

To indicate the effect of the experimentally investigated conditions on the obtained ρapp and ρAr, the measured data are organized in Table 4 depending on each parameter.

Table 4 Measured Apparent and Archimedes Densification for Nickel Pellets of Different Types Arranged According to the Effect of Different Parameters

Parameter	pellet type	ρ_{app}, g/cm^3	ρ_{Ar}, g/cm^3
Effect of particle size	(V)- Ni(B) less than 149 μm	7.40	8.13
	(VI) - Ni(B) less than 70 μm	7.70	8.30
Effect of particles shape	(I)- Ni(A) less than 63 μm	8.24	8.69
	(VI)- Ni(B) less than 70 μm	7.70	8.30
Effect of heating time	(VIII)- 1 h	6.70	8.20
	(IX)- 2 h	7.35	8.30
	(X)- 3 h	7.50	8.33
Effect of the early stage of heating	(IX)- medium	7.35	8.30
	(XI)- slow	7.58	7.60
Effect of wax addition	(I) (wax addition)	8.24	8.69
	(III)	7.43	8.33
	(V) (wax addition)	7.40	8.13
	(VII)	7.03	8.16
Effect of milling	(I)	8.24	8.69
	(II) (tumbling milling)	8.23	8.77

* The milling is carried out in a horizontal ball mill of the smaller size particles Ni(A) for the 4 h at speed of 100 r.p.m.

The densification and porosity are estimated by applying Eqs. 2 and 3, respectively; values obtained are listed in Table 5.

$$\text{Densification} = (\rho app / \rho true) * 100 \qquad (2)$$

$$\text{Porosity} = [(\rho true - \rho)/\rho true] * 100 \qquad (3)$$

where ρ is either ρapp or ρAr while ρtrue is the true density for pure nickel, 8.9 g/cm3 [16].

_____

Table 5 Estimated Densification and Porosity for Different Types of Nickel Pellets

Parameter	Pellet type	Densification estimated based on ρ_{app} (%)	Porosity calculated based on:	
			ρ_{app}, gm/cm^3	ρ_{Ar}, gm/cm^3
Effect of particle size	(V)- Ni(B) less than 149 μm	83.1	16.9	8.6
	(VI) - Ni(B) less than 70 μm	86.5	13.5	6.7
Effect of particles shape	(I)- Ni(A) less than 63 μm	92.6	7.4	2.3
	(VI)- Ni(B) less than 70 μm	86.5	13.3	6.7
Effect of heating time	(VIII)- 1 h	75.3	24.7	7.9
	(IX)- 2 h	82.6	17.4	6.7
	(X)- 3 h	84.3	15.7	6.4
Effect of the early stage of heating	(IX)- medium	82.6	17.4	6.7
	(XI)- slow	85.2	14.8	14.4
Effect of wax addition	(I) (wax addition)	92.6	7.4	2.3
	(III)	83.5	16.5	6.4
	(V) (wax addition)	83.1	16.9	8.6
	(VII)	79.0	21.0	8.3
Effect of milling	(I)	92.6	7.4	2.3
	(II) (tumbling milling)	92.5	7.5	1.5

* The milling is carried out in a horizontal ball mill of the smaller size particles Ni(A) for the 4 h at speed of 100 r.p.m.

Porosity data listed in Table 5 which are estimated based on ρ_{Ar} are lower than values estimated based on ρ_{app}; this might be due to the nature of pores inside the sintered pellets [19]. The difference between both might represent the percentage of open pores which could be filled with the floating liquid (water) used in Archimedes experiments. The open pores percentage of pellets of different types are estimated and listed in Table 6. Accordingly, densification values estimated based on ρ_{Ar} are meaningless.

Table 6 The Open Pores Percentage for Different Types of Nickel Pellets

Pellets type	(I)	(II)	(III)	(IV)	(V)	(VI)	(VII)	(VIII)	(IX)	(X)	(XI)
Open pores (%)	5.1	6	10.1	2.8	8.3	6.9	12.7	16.8	10.7	9.3	0.4
$\dfrac{Open\ Pores\ \%}{Total\ Pores\ \%} x\ 100$	68.9	80.0	61.2	21.4	49.1	51.9	60.5	68.0	61.5	59.2	3

The open pores percentage of pellets of type (XI) is relatively small (0.4%) which might be caused by the slow heating rate at the initial stage of heating the pellets, P(3). This might be due to the acceleration of the initial stage of sintering because of the initial slower heating rate under vacuum which, in turn, caused repulsion of the gaseous phase from pores of the pellets. Therefore, the apparent density obtained for pellets of type (XI) is higher than that of pellets of type (IX) by 3.4%.

3.2.2 Phase Analysis

Fig. 4 shows the XRD patterns obtained from the surface of sintered pellets of types (II) and (XI). Obtained peaks were at angles corresponding to those reported for pure nickel powder [14,15]. Fig. 4 also shows that the intensity of peaks obtained from the surface of a pellet from type (XI) has a higher intensity than those detected from the surface of pellets of type (II). The high intensity might be attributed to the greater randomness of the pellets caused by its smaller grain size.

(a)   (b)
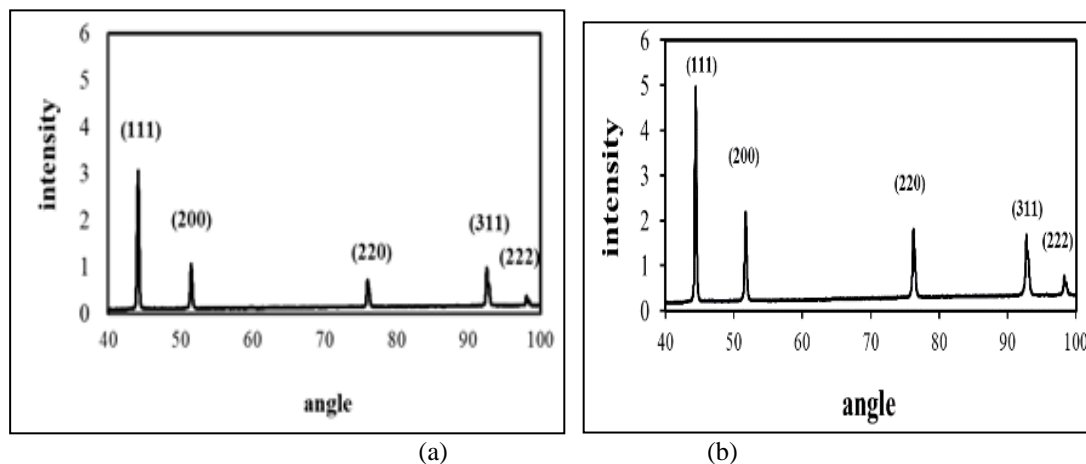
Fig. 4 Typical X-ray diffraction patterns obtained from the surfaces of nickel pellets of type (II) (a) and type (XI) (b)

3.2.3 Microstructural Observation and EDAX Analysis
3.2.3.1 Effect of Wax Addition

The microstructure of types (I), (II) and (V) showed nearly equiaxed grains of a size which varied from 20 to 40 µm for pellets of type (I) and from 10 to 50 µm for pellets of type (II) and from 10 to 30 µm for pellets of type (V).

Fig. (5-a) shows a typical example for the microstructure of a pellet of type (I) shown by scanning electron microscope, at 2000X; the corresponding EDAX results are also shown in the same figure. Many of these grains possessed tiny black particles within their matrix. The EDAX results at most areas of the grains possessed carbon and oxygen peaks with different concentrations, spot (1) as an example, while spot EDAX results obtained from grains that do not include tiny black particles have no peaks of carbon and oxygen spot (2) as an example, as shown in Fig. (5-b). The oxygen% indicator was found to vary from 0.0% to 2.25% while that of carbon varied from 0.0% to 7.7%. The EDAX results of Fig. 6 was obtained by focusing on a tiny black particle of a pellet of type (II) as an example, the carbon% indicator was found to be as high as 24% with no oxygen peaks which means that the tiny black particles were insoluble graphite. It worth noting that the maximum solubility of carbon in nickel is about 0.6 wt% [20].
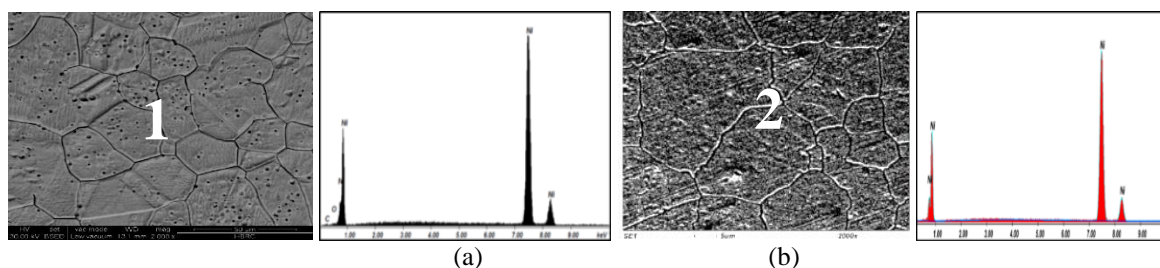

(a)   (b)

Fig. 5 A typical scanning electron micrographs and spot EDAX results for nickel pellets of type (I) at spot (1) (a) and spot (2) (b)

_____

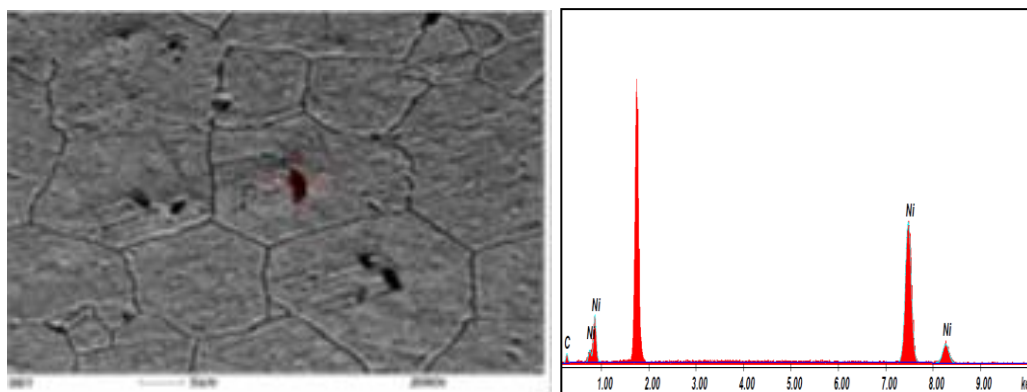*Egypt. J. Chem.* **Vol. 64,** No.1 (2021)

Fig. 6 Scanning electron micrograph and spot EDAX results of nickel pellet type (II) with focusing on a dark spot

Fig. 7 shows the microstructures of pellets of types (I), (II), and (V) which were observed by optical microscopy, at 100X magnification. All microstructures were composed of equiaxed grains but with different shades. This might arises from the variation in the orientation of grains [21]. Many of the grains were found to contain dark graphite particles. The density calculations shed light on the existence of pores between grains which are shown in Fig. 7 as dark areas.
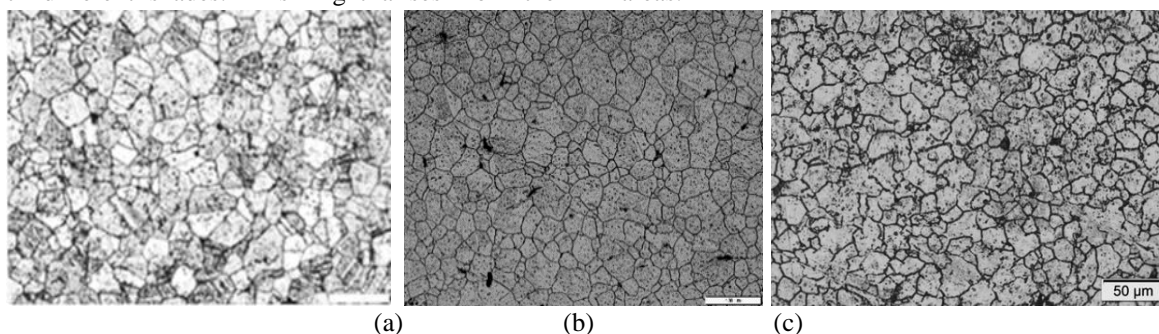

(a)   (b)   (c)

Fig. 7 Optical micrographs for nickel pellets of type (I) (a), type (II) (b) and type (V)

3.2.3.2 Effect of Holding Time at 1200 °C

Fig. 8 represents the SEM micrographs and the corresponding EDAX results of pellets of types (VII), (VIII) and (IX). The EDAX results of pellets of these types indicate the presence of oxygen whose concentration varies between 0.0% and 0.38wt% and the balance is nickel since there is no indication of carbon peaks.
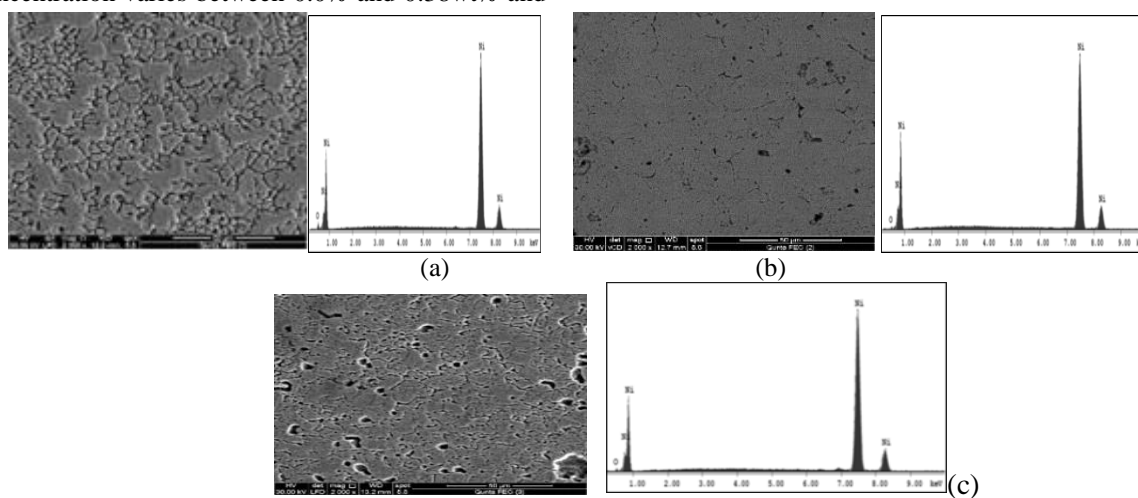

(a)   (b)

(c)

Fig. 8 Scanning electron micrographs and spot EDAX results of nickel pellets at 2000X magnification of type (III) (a), type (IV) (b) and type (V) (c)

_____

Fig. 9 illustrates the optical micrographs that show the microstructures of nickel pellets of types (VII), (VIII) and (IX) which were fabricated at the same preparation conditions and sintering conditions but for different holding time at 1200 °C (1, 2 and 3h, respectively). The figure reveals the formation of dark colonies of equiaxed grains with different heights than the bright regions which surround the dark colonies for pellets of type (VII), Figs. 9(a) and 9(b). The equiaxed grains were a mix of recrystallized and non-recrystallized grains. The non-recrystallized grains were found to be larger than the recrystallized grains which indicated that recrystallization was in its early stage [22]. When the holding time was increased from 1 h to 2 h, the difference in height between various colonies started to decrease; thus the amount of dark regions is reduced as shown in Figs. 9(c) and 9(d) for pellets of type (VIII). Furthermore, the increase of holding time at 1200 °C to 3 h resulted in a further increase in grain size. Figs. 9(e) and 9(f) show that the difference in grains height of pellets of type (IX) is not clear. The largest grain size of pellets of types (VII) and (VIII) was about 5 and 7 µm, respectively, which was much less than the average grain size of Ni(B) particles, 149 µm, which were utilized to prepare pellets of types (VII), (VIII) and (IX). Now, the high-intensity values of the peaks of the XRD patterns obtained from pallets of type (VIII) might be attributed to the greater randomness of pellets of type (VIII) caused by its smaller grain size.
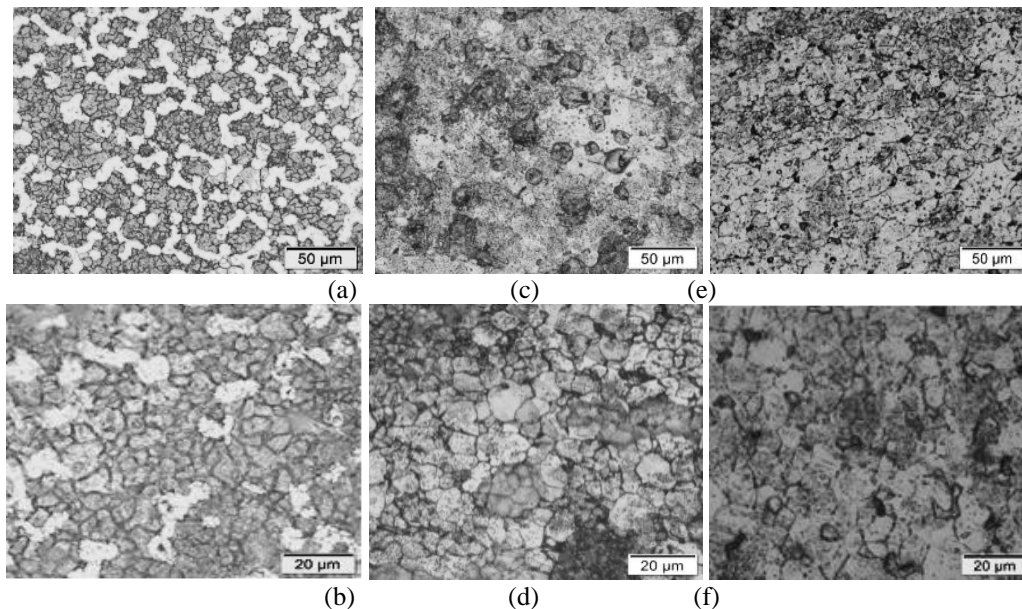

Fig. 9 Optical micrographs for nickel pellets of type (VII) (a and b), type (VIII) (c and d) and type (IX) (e and f)

3.2.3.3 Effect of Slow Heating Rate at the Initial stage of Heating

Fig. 10 shows SEM micrograph of a pellet of type (X) and the corresponding EDAX results; the oxygen% indicator detected in the pellets of type (X) varied from 0.0% to 2.64% which was similar to the oxygen% indicator of pellets of types (I) and (II). No peaks of carbon were detected.
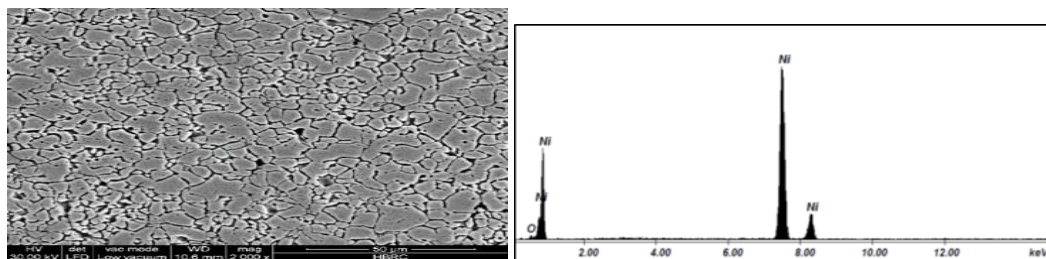

Fig. 10 Scanning electron micrograph and EDAX results for nickel pellets of type (X)

_____

The optical micrograph of a pellet of type (X) is shown in Fig. 11, at 200X magnification. It was noticed that grain refinement took place which might be due to retarding the growth after static recrystallization. Because of static recrystallization, small grains grew along the grain boundaries. The microstructure of pellets of type (X) differed from that of pellets of type (VIII) prepared under the same preparation and sintering conditions except for the heating rate at the early stage of raising the temperature. It was also noticed that non-uniformity in grain size was reduced significantly between the grains of pellets of type (X) as compared to the grains of pellets of type (VIII) [23]. The largest grain size of pellets of type (X) was about 7 µm which is similar to that of pellets of type (VIII).
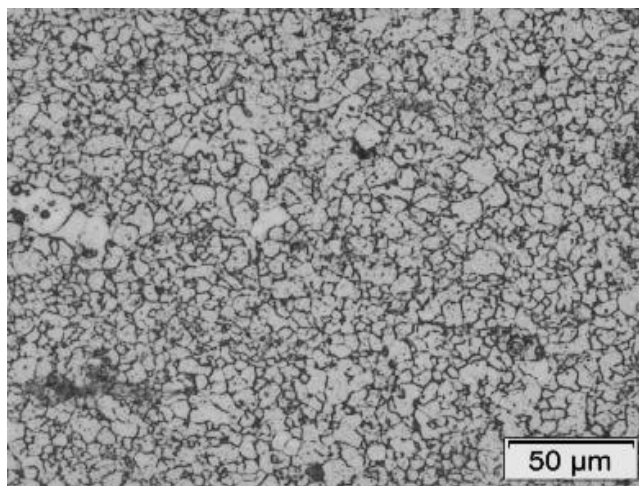

Fig. 11 Optical micrograph for nickel pellets of type (X)

As indicated by EDAX results, pellets of type (X) were found to possess higher oxygen% indicator than that of pellets of type (VIII) which might be due to the slow heating rate at the early stage of heating which allowed more oxygen to diffuse into the pellet producing oxides (mainly NiO). These oxides acted as nucleation sites for static recrystallization and it might retard further growth of recrystallized grains.

Although oxygen% indicator obtained by EDAX results from pellets of types (I) and (II) was close to that of pellets of type (X), the grain growth was more pronounced in pellets of types (I) and (II) than that of pellets of type (X). This might be caused by the disability of oxygen to form oxides in the pellets of types (I) and (II) because of the presence of graphite spots. Besides, grain growth retardation might be caused by the higher porosity content in pellets of type (X) which acted as a barrier for further growth of grains. The strain fields result from these pores retarded the grain boundary migration and, in turn, grain refinement occurred. Pores might also act as energy sink which might cause a reduction of energy that should be provided for further growth of recrystallized grains.

3.2.4 Microhardness Measurements

Table 7 presents the average microhardness values of pellets of different types. During the conventional powder metallurgy process, uniaxial compaction activates more slip systems, thus strain fields are produced due to dislocation interactions which increase pellet hardness[22]. Pellets of types (I) and (II) prepared from filamentary particles, Ni(A), with 0.5 wt% wax addition as a binder were found to have similar hardness values which were found to be higher than those obtained from pellets produced from Ni(B) powder without the addition of any binder. An increase in the average microhardness value from 68 VHN to 100 VHN was observed when the holding time at 1200 °C was increased from 1 h to 3 h (pellets of types (VII), (VIII) and (IX)). It is clear that the nickel particle shape, size, and the holding time at 1200 °C were the most important parameters affecting the microhardness of the sintered pellets; this trend is similar to previous results [24].

_____

Table 7 Microhardness for Different Types of Nickel Pellets

Parameter	Pellet type	Microhardness, VHN
Effect of particle size	(V)	90
	(VI)	92
Effect of particles shape	(I)	155
	(VI)	92
Effect of heating time	(VIII)- 1 h	68
	(IX)- 2 h	91
	(X)- 3 h	100
Effect of the early stage of heating	(IX)- medium	91
	(XI)- slow	73
Effect of addition of wax	(I)	155
	(III)	149.1
	(V)	90
	(VII)	95
Effect of milling	(I)	155
	(II)	161

* The milling is carried out in a horizontal ball mill of the smaller size particles Ni(A) for the 4 h at speed of 100 r.p.m.

4. Conclusion

The effect of shape and size of nickel particles, wax addition as a binder, milling for 4 h, the rate of rising temperature at the early stage of heating from room temperature up to 300 °C and holding time at the sintering temperature of 1200 °C on the apparent density, microstructure and microhardness of sintered pellets are experimentally investigated. Pellets prepared from filamentary nickel particles with particle size less than 63 µm have higher apparent density values than that of pellets prepared from nearly spherical shape particles with particle size less than 149 µm and no-wax addition. Increasing the holding time at 1200 °C increases the densification of pellets prepared from nearly spherical particles with no binder under the same preparation conditions. Pellets prepared at a lower rate of raising temperature at the early stage of heating have densification value and a negligible percentage of open pores than pellets prepared under the same conditions but with higher heating rate at the early heating stage. The matrix of all pellets of different types consists of equiaxed grains with larger grain size of pellets. These pellets are prepared from filamentary particles of smaller size than the grain size of pellets prepared from larger-size particles. These larger size are nearly spherical particles formed as a result of static recrystallization.

Graphite tiny black particles are formed within many of the nickel grains of the sintered pellets prepared from filamentary particles. Closed and open pores are noticed because of the addition of 0.5 wt% wax as a binder. Both particles are detected with the formation of a minimum open pores if the pellets are heated with slower rate-raising temperature from room temperature to 300 °C. The micro hardness of pellets prepared under the same preparation conditions increases as the holding time at the sintering temperature of 1200 °C increases. The micro hardness is therefore, increases as the porosity decreases. Finally, the main conclusions of this paper are:

1. The pellets made from Ni(A) powder have a higher densities and microhardness than the pellets made from Ni(B) powder.
2. The heating program (P1) gives best properties for the pellets made from Ni(A) powder. However, the heating program (P2) provides a good properties of pellets made from Ni(B) powder.

5. Acknowledgments

_____

6. Conflicts of interest

There are no conflicts to declare.

7. References

[1] Mohamed L.Z., El Kady O.A., Lotfy M.M., Ahmed H.A., Elrefaie F.A., Characteristics of Ni-Cr binary alloys produced by conventional powder metallurgy, Key Eng. Mater., 835, 214-222 (2020)

[2] Xue M., High temperature oxidation and wear behavior of powder metallurgically developed Ni-Cr-W-Al-Ti-MoS2 composite, Indian J Eng Mater Sci, 16, 111-115 (2009)

[3] Zheng L., Zhang M., Dong J., Oxidation behavior and mechanism of powder metallurgy Rene95 nickel based superalloy between 800 and 1000 °C, Appl Surf Sci, 256, 7510–7515 (2010)

[4] Chao-Gjie W., Tao Y., Jia J., Microstructure and properties of an advanced nickel-base PM superalloy, J. Iron Steel Res Int, 12, 1152-1157 (2014)

[5] Erdem M., Turker M., High temperature oxidation behavior of a Ni based superalloy produced by mechanical alloying, Sci. Res. Essays, 7, 4123-4129 (2012)

[6] Hardy M.C., Herbert C.R.J., Kwong J., Li W., Axinte D.A., Sharman A.R.C., Encinas-Oropesa A., Withers P.J., Characterizing the integrity of machined surfaces in a powder nickel alloy used in aircraft engines, Procedia CIRP, 13, 411 – 416 (2014)

[7] Bai Q., Lin J., Tian G., Zou J., and Dean TA., Review and analysis of powder prior boundary (PPB) formation in powder metallurgy processes for nickel-based super alloys, Review Article, J Powder Metall Min, 4-1 (2015)

[8] Mohamed L.M., Ghanem W.A., El kady O.A., Lotfy M.M., Ahmed H.A., Elrefaie F.A., Oxidation characteristics of porous-nickel prepared by powder metallurgy and cast-nickel at 1273K in air for total oxidation time of 100 h, J. Advan. Res., 8, 717-729 (2017)

[9] C.H. Zhou C.H., Pan R.Y., Zhang H., Guan X.G., Oxidation Behavior of Ni-10Cr Alloy under the Compressive Stress at 900 °C, 3rd Asia-Pacific Electronics and Electrical Eng. Conf., (2018)

[10] Chou k, Luo Q, Li Q, Zhang J, Influence of the density of oxide on oxidation kinetics, Intermetallics, 47, 17-22 (2014)

[11] R. Haugsrud, On the high-temperature oxidation of nickel, Corros Sci, 45, 211–235 (2003)

[12] Mohammed M.M.M., Elkady O.A., Abdelhameed A. W., High nickel alloys offering a combination of high strength and high impact properties, Open J Metal, 3, 72-79 (2013)

[13] Lippold J.C., kiser S.D., Welding metallurgy and weldability of nickel-base alloys, 420 (2003)

[14] Bayliss P., Erd D.C., Mrose M.E., Sabina A.P., Smith D.K., Mineral powder diffraction file-data book, (1986)

[15] Swanson, Tatge., Natl. Bur. Stand. (U.S.), Circ. 539, I (13), (1953)

[16] Lee P.W., ASM Handbook: Powder metal technologies and applications, 7, (2004)

[17] Somiya S, Aldinger F, Claussen N, Spriggs R.M, Uchino K, Koumoto K, Kaneno M, Handbook of Advanced Ceramics: Vo. II Processing and their Applications, (2003)

[18] Kofstad P., Non-stoichiometry diffusion and electrical conductivity in binary metal oxides, 109-113 (1972)

[19] Bergman O., Key aspects of sintering powder metallurgy steel prealloyed with chromium and manganese, Ph.D., Gothenburg, Sweden, (2011)

[20] Edward H. Kottcamp, Jr., Edward L. Langer., ASM Handbook: Alloy phase diagrams, 3 (2004)

[21] George F., Voort V., ASM Handbook: Metallography and microstructures, 9 (2004)

[22] Hasgawa M., Fukutomi H., Microstructure evolution of polycrystalline pure nickel during static recrystallization, Mater Trans, 43(9), 2243-2248 (2002)

[23] Hostlzler R., Flasgov T., Recrystallization characteristics of oxide dispersion strengthened nickel-based alloys, Superalloys Conf, Fourth International Symposium, 455-464 (1980)

[24] Delavari M., Salarvand A., Rahi A., Shahri F., The effect of powder metallurgy process parameters on mechanical properties of Micro and nano-iron powder, Int J Eng Sci Technol, 3(9), 86-94 (2011)